Spectroscopic Observations of Mercury's Surface Reflectance During MESSENGER's First Mercury Flyby

William E. McClintock, *et al.*

Science **321**, 62 (2008);
DOI: 10.1126/science.1159933

Fe abundance is less than ~6% and would be lower still if Ti, Gd, or Sm is present. For comparison, the average Fe abundance is about 5% and 8% in Earth's continental and oceanic crust, respectively, and 5% in lunar highlands crust (*33*).

During its flyby, MESSENGER provided a comprehensive view of solar wind interaction with Mercury's magnetic field and neutral atmosphere and, indirectly, its surface. At the time of the flyby, solar activity was low and, in contrast with Mariner 10 observations, no energetic charged particles with energies above ~30 keV were detected (*34*). Magnetometer observations (*14*) of the magnetospheric boundaries, current systems, and plasma waves confirm that this magnetosphere appears structurally to be a miniature of that of Earth. One notable difference is the presence of a double current sheet at the dawn terminator that likely represents heavy planetary ion effects unique to Mercury (*34*). The Mercury Atmospheric and Surface Composition Spectrometer observed neutral Na and Ca in Mercury's exosphere—delivered from surface materials in part by the same micrometeoroid and ion-impact processes that space-weather the surface—and mapped the structure of Mercury's antisunward Na tail (*35*). The Fast Imaging Plasma Spectrometer sensor on the Energetic Particle and Plasma Spectrometer instrument (*36*) observed a range of heavy magnetospheric plasma ions—including O^+, Na^+, Mg^+, K^+, Ca^+, S^+, and H_2S^+—derived from the exosphere or surface (*37*). On the basis of the full set of observations made during MESSENGER's first flyby, Mercury is seen to be a dynamic planet where the interactions among core, surface, exosphere, magnetosphere, and interplanetary environment are strongly interlinked (Fig. 6). Subsequent encounters under different solar conditions and one Earth year in orbit about Mercury as the Sun approaches the next maximum in the solar cycle should permit MESSENGER to explore these interactions across their full range of behavior.

References and Notes

1. S. C. Solomon, *Earth Planet. Sci. Lett.* **216**, 441 (2003).
2. H. Harder, G. Schubert, *Icarus* **151**, 118 (2001).
3. P. D. Spudis, J. E. Guest, in *Mercury*, F. Vilas, C. R. Chapman, M. S. Matthews, Eds. (Univ. of Arizona Press, Tucson, 1988), pp. 118–164.
4. J. L. Margot, S. J. Peale, R. F. Jurgens, M. A. Slade, I. V. Holin, *Science* **316**, 710 (2007).
5. N. F. Ness, K. W. Behannon, R. P. Lepping, Y. C. Whang, *J. Geophys. Res.* **80**, 2708 (1975).
6. B. C. Murray, *J. Geophys. Res.* **80**, 2342 (1975).
7. S. C. Solomon, R. L. McNutt Jr., R. E. Gold, D. L. Domingue, *Space Sci. Rev.* **131**, 3 (2007).
8. J. V. McAdams, R. W. Farquhar, A. H. Taylor, B. G. Williams, *Space Sci. Rev.* **131**, 219 (2007).
9. S. E. Hawkins III *et al.*, *Space Sci. Rev.* **131**, 247 (2007).
10. S. Stanley, J. Bloxham, W. E. Hutchison, M. T. Zuber, *Earth Planet. Sci. Lett.* **234**, 27 (2005).
11. M. H. Heimpel, J. M. Aurnou, F. M. Al-Shamali, N. Gomez Perez, *Earth Planet. Sci. Lett.* **236**, 542 (2005).
12. U. R. Christensen, *Nature* **444**, 1056 (2006).
13. O. Aharonson, M. T. Zuber, S. C. Solomon, *Earth Planet. Sci. Lett.* **218**, 261 (2004).
14. B. J. Anderson *et al.*, *Science* **321**, 82 (2008).
15. B. Chen, J. Li, S. A. Hauck II, *Geophys. Res. Lett.* **35**, L07201, 10.1029/2008GL033311 (2008).
16. R. G. Strom, N. J. Trask, J. E. Guest, *J. Geophys. Res.* **80**, 2478 (1975).
17. T. R. Watters, M. S. Robinson, A. C. Cook, *Geology* **26**, 991 (1998).
18. S. A. Hauck II, A. J. Dombard, R. J. Phillips, S. C. Solomon, *Earth Planet. Sci. Lett.* **222**, 713 (2004).
19. S. L. Murchie *et al.*, *Science* **321**, 73 (2008).
20. R. G. Strom, C. R. Chapman, W. J. Merline, S. C. Solomon, J. W. Head III, *Science* **321**, 79 (2008).
21. J. W. Head *et al.*, *Science* **321**, 69 (2008).
22. M. S. Robinson, G. J. Taylor, *Meteorit. Planet. Sci.* **36**, 841 (2001).
23. M. T. Zuber *et al.*, *Science* **321**, 77 (2008).
24. W. V. Boynton *et al.*, *Space Sci. Rev.* **131**, 85 (2007).
25. W. E. McClintock *et al.*, *Science* **321**, 62 (2008).
26. M. S. Robinson *et al.*, *Science* **321**, 66 (2008).
27. B. Hapke, *J. Geophys. Res.* **106**, 10039 (2001).
28. J. O. Goldsten *et al.*, *Space Sci. Rev.* **131**, 339 (2007).
29. W. C. Feldman *et al.*, *J. Geophys. Res.* **105**, 20347 (2000).
30. W. C. Feldman, D. M. Drake, *Nucl. Instrum. Methods Phys. Res. A* **245**, 182 (1986).
31. D. J. Lawrence *et al.*, *J. Geophys. Res.* **111**, E08001, 10.1029/2005JE002637 (2006).
32. L. Haskin, P. Warren, in *Lunar Sourcebook*, G. Heiken, D. Vaniman, B. M. French, Eds. (Cambridge Univ. Press, New York, 1991), pp. 357–474.
33. K. Lodders, B. Fegley Jr., *The Planetary Scientist's Companion* (Oxford Univ. Press, New York, 1998), pp. 140 and 177.
34. J. A. Slavin *et al.*, *Science* **321**, 85 (2008).
35. W. E. McClintock *et al.*, *Science* **321**, 92 (2008).
36. G. B. Andrews *et al.*, *Space Sci. Rev.* **131**, 523 (2007).
37. T. H. Zurbuchen *et al.*, *Science* **321**, 90 (2008).

38. The hundreds of engineers and technical support personnel who brought MESSENGER from a concept to a successful flight project warrant the sustained appreciation of the mission science team. We also thank L. M. Prockter for assembling fig. S1. The MESSENGER project is supported by the NASA Discovery Program under contracts NASW-00002 to the Carnegie Institution of Washington and NAS5-97271 to Johns Hopkins University Applied Physics Laboratory.

Supporting Online Material

www.sciencemag.org/cgi/content/full/321/5885/59/DC1
Fig. S1
References

28 April 2008; accepted 3 June 2008
10.1126/science.1159706

REPORT

Spectroscopic Observations of Mercury's Surface Reflectance During MESSENGER's First Mercury Flyby

William E. McClintock,[1]* Noam R. Izenberg,[2] Gregory M. Holsclaw,[1] David T. Blewett,[2] Deborah L. Domingue,[2] James W. Head III,[3] Jörn Helbert,[4] Timothy J. McCoy,[5] Scott L. Murchie,[2] Mark S. Robinson,[6] Sean C. Solomon,[7] Ann L. Sprague,[8] Faith Vilas[9]

During MESSENGER's first flyby of Mercury, the Mercury Atmospheric and Surface Composition Spectrometer made simultaneous mid-ultraviolet to near-infrared (wavelengths of 200 to 1300 nanometers) reflectance observations of the surface. An ultraviolet absorption (<280 nanometers) suggests that the ferrous oxide (Fe^{2+}) content of silicates in average surface material is low (less than 2 to 3 weight percent). This result is supported by the lack of a detectable 1-micrometer Fe^{2+} absorption band in high-spatial-resolution spectra of mature surface materials as well as immature crater ejecta, which suggests that the ferrous iron content may be low both on the surface and at depth. Differences in absorption features and slope among the spectra are evidence for variations in composition and regolith maturation of Mercury's surface.

Before MESSENGER's first flyby of Mercury on 14 January 2008, our knowledge of the planet's surface mineralogy came from low-spatial-resolution, ground-based spectroscopic observations. Early disk-integrated observations showed a low-albedo, relatively featureless spectrum that increases monotonically across the visible to near-infrared wavelengths, a characteristic referred to as a "red" spectral slope (*1*–*3*). On the Moon these spectral characteristics result from space weathering, a process in which amorphous silica coatings containing nanometer-scale metallic iron (nanophase metallic iron, $npFe^0$) darken exposed regolith, increase spectral slope, and reduce spectral contrast (*4*, *5*). Although Mercury's surface appears to be highly space-weathered, the absence of identifiable near-infrared absorptions argues for a low average ferrous iron content (*2*, *6*, *7*). This view is supported by recent mid-infrared emission spectra and reflectance observations that have been interpreted to indicate the presence of plagioclase feldspar and low-iron orthopyroxene (enstatite) (*6*, *8*, *9*) and high-Ca clinopyroxene (*10*). These mid-infrared spectra support the presence of Na-bearing feldspar and Mg-rich minerals (*8*), which are present in very-low-iron terrestrial rock types. To more fully understand Mercury's surface composition, it is necessary to explore regional spectral variations across units that contain relatively unweathered materials, such as ejecta from small craters, which are often less than 100 km

in diameter. This has not been possible from Earth because long atmospheric path lengths and low spatial resolution (>200 km) hinder the observations.

During MESSENGER's flyby, the Mercury Atmospheric and Surface Composition Spectrometer (MASCS) (*11*) measured high-spatial-resolution reflectance spectra from Mercury's surface. MASCS consists of a small Cassegrain telescope that simultaneously feeds a Visible and Infrared Spectrograph (VIRS) and an Ultraviolet and Visible Spectrometer (UVVS), covering the wavelengths 325 to 1300 nm and 220 to 320 nm, respectively. Both VIRS (0.023° circular field of view) and UVVS (0.04° × 0.05° rectangular field of view) are point instruments whose fields of view (FOVs) are offset by 0.38° in the telescope focal plane. The MESSENGER observations constitute the first reflectance measurements at high spatial and high spectral resolution, as well as the first middle ultraviolet (MUV) spectra (220 to 350 nm), of Mercury's surface.

Nine days after closest approach, MASCS obtained full-disk spectra of Mercury at a phase angle of 87° and a planetary diameter of 0.068°. In Fig. 1A, these are compared with spectra of the southern hemisphere of the lunar farside—which contains feldspathic highlands, the interior of the South Pole–Aitken Basin, and some maria—obtained by MASCS on 31 July 2005. Observations using a single spacecraft instrument and similar viewing geometry allow us to compare directly the reflectance of Mercury's surface to that of the Moon, which has been extensively studied using both remote sensing techniques and laboratory analysis of soil and rock samples acquired during the Apollo and Luna programs. To facilitate direct comparison, we used an empirical multispectral phase function of the Moon derived from Robotic Lunar Observatory (ROLO) observations (*12*) to adjust the MASCS lunar spectrum to 87° phase angle.

The MASCS disk-averaged spectra of Mercury and the Moon display the characteristic red slope at visible wavelengths (350 to 600 nm) observed from Earth (*3*, *12*); however, Mercury's visible spectral slope is 10% less than that of the Moon. The shallower slope continues into the infrared, but the difference becomes less pronounced (*13*). Throughout the MUV, the lunar spectrum obtained by MASCS is also observed to increase in a nearly linear fashion (Fig. 1B). This linear trend is present in spectra of the lunar nearside obtained from Earth orbit (*14*, *15*) and in laboratory spectra of returned lunar soil samples (*16*). In contrast, Mercury's disk-averaged MUV (<300 nm) reflectance displays an abrupt downturn toward shorter wavelengths relative to the linear-sloped visible trend. This downturn is also observed in the spatially resolved UV spectrum of a crater filled with smooth plains material (location A in Fig. 2).

Laboratory spectra of lunar rock powders exhibit strong trough-like features (*16*) that result from the presence of oxygen–transition metal charge transfer (OMCT) bands, which are the main cause for absorption in silicate materials at wavelengths of 200 to 400 nm (*17*, *18*). Trough-like features are not observed in UV spectra of the lunar nearside taken from Earth orbit (*14*, *15*) or in laboratory spectra of both mature and immature lunar soils (*16*) because of space weathering by micrometeorite impacts and solar wind sputtering. A primary mechanism causing suppression of UV bands is the reduction of ferrous iron followed by the vapor deposition of a npFe^0-rich patina (*4*, *19*–*21*). This patina masks the UV absorption within the underlying silicate material and erodes the long-wavelength absorption edge, producing a spectrum with a nearly linear slope extending to visible wavelengths (*4*, *22*), and substantially reduces the contrast observed in Fe^{2+} bands that occur in the infrared near 1 μm.

The location of the downturn in Mercury's spectrum, with its edge near 280 nm (>20% depression below the linear continuum), and its troughlike long-wavelength shoulder are consistent with the presence of OMCT bands caused by Fe^{2+} and/or Ti^{4+}, which have band centers near 250 nm (*18*, *23*). Furthermore, the depth and shape of the band argue that the ferrous iron content is low in the average surface materials. Laboratory UV reflectance spectra show that the inclusion of even 2 to 3 weight percent Fe^{2+} in silicates (*24*) and glasses (*25*) results in a deep central absorption and a movement of the absorption edge from 270 nm toward 300 nm. An OMCT feature due to Fe^{2+} can be present at 250 nm even if iron abundance were too low to produce a detectable

[1]Laboratory for Atmospheric and Space Physics, University of Colorado, Boulder, CO 80303, USA. [2]Johns Hopkins University Applied Physics Laboratory, Laurel, MD 20723, USA. [3]Department of Geological Sciences, Brown University, Providence, RI 02912, USA. [4]Institute of Planetary Research, Deutsches Zentrum für Luft- und Raumfahrt, Berlin 12489, Germany. [5]National Museum of Natural History, Smithsonian Institution, Washington, DC 20560, USA. [6]Department of Geological Sciences, Arizona State University, Tempe, AZ 85287, USA. [7]Department of Terrestrial Magnetism, Carnegie Institution of Washington, Washington, DC 20015, USA. [8]Lunar and Planetary Laboratory, University of Arizona, Tucson, AZ 85721, USA. [9]MMT Observatory, University of Arizona, Tucson, AZ 85721, USA

*To whom correspondence should be addressed. E-mail: william.mcclintock@lasp.colorado.edu

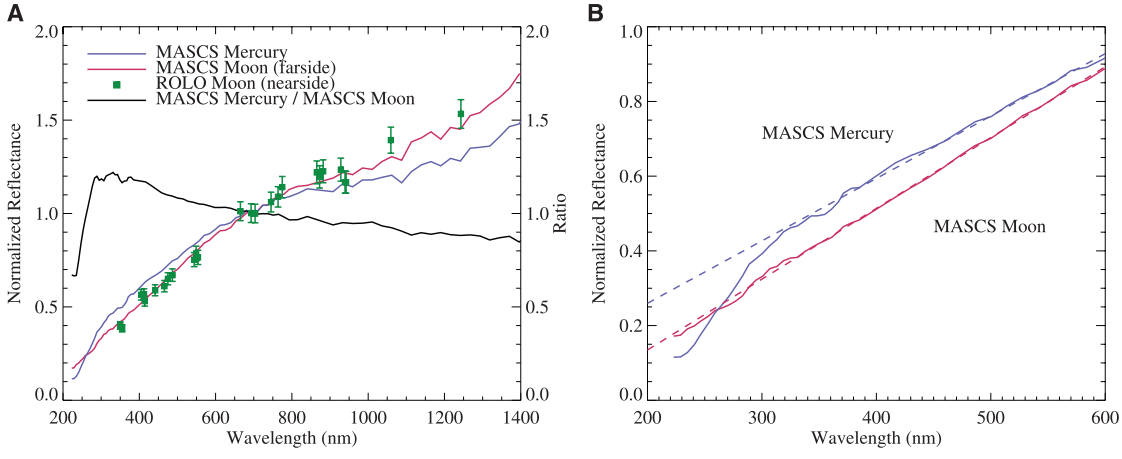

Fig. 1. (**A**) MASCS disk-averaged reflectance (observed spectral radiance of the surface divided by the radiance from a hypothetical normally illuminated Lambertian disk) of Mercury and the Moon, along with a ROLO-derived full-disk spectrum of the waxing phase (87°) of the lunar nearside, which is predominantly composed of highlands terrain. These spectra are scaled to a value of 1.0 at 700 nm. The excellent agreement between the adjusted MASCS lunar observations and the ROLO spectrum provides confidence in the instrument radiometric performance and a reference for interpreting the Mercury data. The ratio of Mercury reflectance to that of the Moon highlights the differences between the spectral properties of the two bodies. (**B**) Mercury's MUV reflectance (blue curve) exhibits a distinct departure from a linear trend (blue dashed line) at wavelengths <300 nm that is not observed for the Moon (red curved and dashed line).

band near 1 μm, because the OMCT band arises from a strong, allowed transition, whereas the near-infrared band is a forbidden (and thus weak) transition (*17*). Assemblages containing iron-poor pyroxene or olivine, or plagioclase feldspar with small amounts of iron, produce laboratory UV absorption spectra consistent with the current data (*24*). These mineralogical interpretations are similar to those made from ground-based mid-infrared spectra of Mercury (*26*). Ti^{4+} could also produce an OMCT feature near 250 nm without exhibiting a corresponding 1-μm band. Because Fe^{2+} abundance in silicates appears to be very low for the surfaces observed by MASCS, nonsilicate phases such as iron-bearing opaque minerals (*27*) and sulfides or meteoritic infall (*28*) could provide the source of the nanometer-scale metallic particles that darken and redden Mercury's spectrum.

If the vapor-deposited metallic particles are <25 nm in diameter, then the presence of a trough-like OMCT feature in Mercury's spectrum limits the amount of $npFe^0$ (or possibly nanometer-scale Ti^0 particles, which have virtually identical optical absorption properties) in the patinas and coatings of surface materials to 0.1 to 0.2 weight percent, because larger amounts produce broad UV absorptions that would erode the shape of bands (*4*). Laboratory experiments with regolith analogs indicate that larger particle size tends to lower reflectance throughout the visible and near-infrared with little change in overall shape (*22*). The size range for metallic iron particles that contribute to space weathering effects in lunar soils may vary from a few nanometers to hundreds of nanometers, but $npFe^0$ size on Mercury may be different. More intense micrometeoritic bombardment is expected at Mercury than at the Moon (*29*). Furthermore, Ostwald ripening—a process by which $npFe^0$ particles within a glass matrix coarsen at elevated temperature—could also be operating on Mercury (*28*). Recent analysis of Mariner 10 (*30*) and MESSENGER (*31*) multispectral images provides evidence that relatively coarse-grained opaque phases (i.e., particle diameters

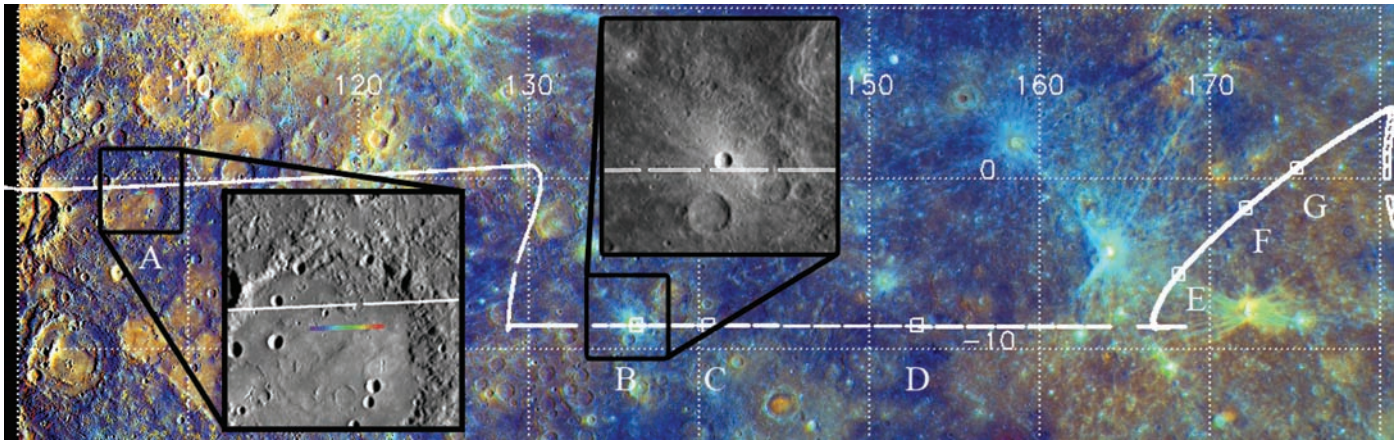

Fig. 2. A segment of the VIRS FOV track is shown in white over an MDIS image mosaic, formed by combining a high-resolution narrow-angle camera (NAC) image mosaic with a lower-resolution color image composite (*31*). MDIS images reveal a surface populated by three major color units: higher-reflectance, relatively red smooth plains; lower-reflectance material with lesser spectral slope; and intermediate material. The first part of the track crosses primarily intermediate terrains before briefly entering the northern edge of a relatively young smooth plains unit (near G) identified in MDIS color images. Locations B to G along the track correspond to the spectra shown in Fig. 3. The spatial-spectral sampling of UVVS is denoted by a rainbow for the single spectrum taken during the flyby.

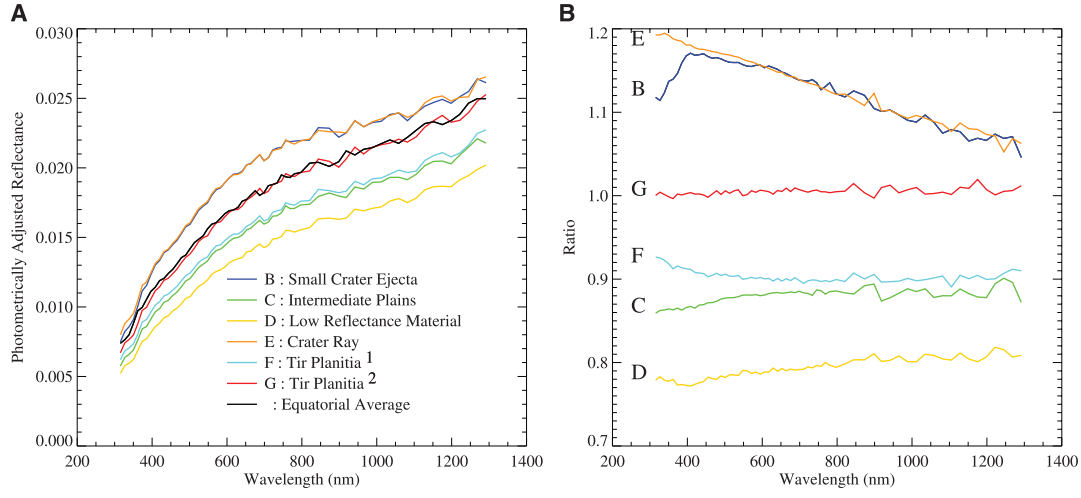

Fig. 3. (**A**) Spectra B and C are from the bright ejecta of an impact crater ~10 km in diameter (8.5°S, 136.3°E) and from an intermediate plains unit just east of the crater, respectively (see Fig. 2). Spectrum D is from low-reflectance material (8.6°S, 154.7°E). Spectrum E is from an area where a bright crater ray overlays a smooth plains unit (5.6°S, 168.2°E). Spectra from plains units (F and G) adjacent to and within Tir Planitia (3°S, 177°E) are also shown. All were adjusted to a common viewing geometry (i = 73° and e = 14.5°) and plotted on a common vertical scale. Thus, differences in magnitude and shape represent real variation in surface reflectance properties from location to location. (**B**) Ratios of the spectra shown in (A) to the average MASCS surface spectrum highlight spectral differences.

greater than that of npFe^0) play an important role in albedo and color variations on Mercury. The low, featureless reflectance typical of opaque minerals, such as ilmenite, is known to decrease the overall reflectance of a mixture and decrease its spectral slope (*27*), so a larger abundance of an opaque phase in Mercury's surface relative to that on the Moon could explain the low reflectance and the visible-infrared spectral slope.

Spatially resolved MASCS observations began near 0°N, 95°E, as the spacecraft crossed the morning terminator and continued to about 10°S, 180°E (Fig. 2). During this traverse, the FOVs primarily crossed terrains identified in Mercury Dual Imaging System (MDIS) color images (*31*) as units with intermediate reflectance, but they also sampled some low-reflectance units. The combination of spacecraft motion and changing distance to the surface caused the VIRS spectral footprint to vary from 1 × 5 km to 2 × 75 km (caused by a spacecraft slew) and back to 2 × 5 km along the ground track. All of the spectra were acquired at phase angles of ~90°, with incidence angle (i) beginning at 80° and ending at 10°. Operational constraints limited the UVVS observations to a single usable spectrum, with footprint dimensions of 1 km × 40 km, acquired while the instrument FOV crossed a smooth-floored crater near 1°S, 107°E (i = 78°). During each integration period, VIRS simultaneously records the magnitude of reflected light across all wavelengths within its spatial FOV; in contrast, UVVS builds a spectrum by scanning through wavelengths as the spatial FOV moves across the surface. The VIRS and UVVS FOV tracks are offset by 16 km at this location.

Example spectra (Fig. 3A), adjusted to a common viewing geometry by means of a Hapke photometric model (*32*), provide insight into regolith compositional differences and maturation processes on Mercury. Ratios of these spectra to an average of 492 spectra with $i < 75°$ and emission angle $e < 75°$ (Fig. 3B) highlight subtle spectral variations. Compositional variation on small scales is evidenced in the near-UV portion of the spectrum. In relatively fresh materials, the striking difference between the small crater ejecta spectrum (B) and the crater ray spectrum (E) below 400 nm (Fig. 3B) likely reflects a compositional difference between the two locations and is not solely an effect of differential maturity. Slope and curvature differences in both the visible and near-infrared among the spectra of surfaces of roughly similar maturity (C, D, F, and G, Fig. 3B) are also suggestive of compositional differences. In particular, the upturn seen below 500 nm in the low-reflectance material (D) is consistent with the presence of ferrous iron- and titanium-bearing opaque phases at that location (*31*), as seen in the spectra of some opaque-rich returned lunar samples (*16*). An equally suggestive, more pronounced, upturn is also seen in the spectrum at F—which appears in MDIS images to be a mixture of low-reflectance and intermediate materials—but is conspicuously absent in the nearby spectrum at G, which is primarily composed of intermediate material. Because spectral slope and band depth change not only with composition but also with soil grain size, detailed radiative transfer modeling will be needed to constrain the specific mineral phases present.

Lunar-like maturity trends are also clearly evident in the MASCS data. The small crater (B, Figs. 2 and 3A) and the bright ray (E, Figs. 2 and 3A) represent stratigraphically young, fresh material. Their relative spectra have negative slopes and relatively high reflectance, whereas the older mature units have a positive slope and low reflectance, commensurate with the darkening and reddening associated with space weathering. The small crater (B) shows an enhanced absorption at wavelengths less than 400 nm relative to both the adjacent plains unit (C) and the average equatorial terrains. Because the crater and the adjacent plains are likely to have the same composition, this difference could indicate that the OMCT UV band in the more mature plains material has been more obscured by space weathering, causing spectra B and C to differ in the same way as spectra for a powdered lunar rock differ from those of a lunar soil (as described earlier). This discovery indicates that the spectral shape in the near-UV may be a useful indicator of optical maturity. None of the VIRS spatially resolved spectra exhibit a 1-μm absorption band (*33*), including the freshest material. Therefore, it is very unlikely that the ferrous iron absorption on Mercury has been hidden or erased by intense space weathering (*29*). The absence of this band is further evidence that ferrous iron is only minimally present in silicates, both on the surface and at depth within the crust, in the regions sampled by MASCS.

References and Notes

1. T. B. McCord, J. B. Adams, *Icarus* **17**, 585 (1972).
2. F. Vilas, *Icarus* **64**, 133 (1985).
3. F. Vilas, in *Mercury*, F. Vilas, C. R. Chapman, M. S. Matthews, Eds. (Univ. of Arizona Press, Tucson, AZ, 1988), pp. 59–76.
4. B. Hapke, *J. Geophys. Res.* **106**, 10039 (2001).
5. E. M. Fischer, C. M. Pieters, *Icarus* **111**, 475 (1994).
6. B. Hapke, G. E. Danielson Jr., K. Klaasen, L. Wilson, *J. Geophys. Res.* **80**, 2431 (1975).
7. J. Warell, *Icarus* **161**, 199 (2003).
8. A. L. Sprague, T. L. Roush, *Icarus* **133**, 174 (1998).
9. J. Warell, D. T. Blewett, *Icarus* **168**, 257 (2004).
10. J. Warell, A. L. Sprague, J. P. Emery, R. W. H. Kozlowski, A. Long, *Icarus* **180**, 281 (2006).
11. W. E. McClintock, M. R. Lankton, *Space Sci. Rev.* **131**, 481 (2007).
12. H. H. Kieffer, T. C. Stone, *Astron. J.* **129**, 2887 (2005).
13. Prior comparisons of the slope of ground-based Mercury spectra (expressed as the ratio of reflectance at 415 nm to that at 750 nm) to that of the Moon (*34*) did not find a consistent relation. We argue that the observations reported here, made with the same instrument and free from the complicating effects of the terrestrial atmosphere and stellar calibrations, are more reliable.
14. S. Janz, E. Hilsenrath, R. Cebula, T. Kelly, *Geophys. Res. Lett.* **23**, 2297 (1996).
15. G. K. Fox *et al.*, *Mon. Not. R. Astron. Soc.* **298**, 303 (1998).
16. J. K. Wagner, B. W. Hapke, E. N. Wells, *Icarus* **69**, 14 (1987).
17. R. G. Burns, in *Remote Geochemical Analysis*, C. Pieters, P. Englert, Eds. (Cambridge Univ. Press, Cambridge, 1993), pp. 3–29.
18. J. A. Tossell, D. J. Vaughn, K. H. Johnson, *Am. Mineral.* **59**, 319 (1974).
19. B. Hapke, W. Cassidy, E. Wells, *Moon* **13**, 339 (1975).
20. B. Hapke, *Phys. Earth Planet. Inter.* **15**, 264 (1977).
21. C. M. Pieters *et al.*, *Meteorit. Planet. Sci.* **35**, 1101 (2000).
22. S. K. Noble, C. M. Pieters, L. P. Keller, *Icarus* **192**, 629 (2007).
23. B. M. Loeffler *et al.*, *Geochim. Cosmochim. Acta* **3** (suppl. 5), 3007 (1974).
24. E. A. Cloutis *et al.*, *Icarus*, 10.1016/j.icarus.2008.04.018 (2008).
25. E. Wells, B. Hapke, *Science* **195**, 977 (1977).
26. A. L. Sprague *et al.*, *Meteorit. Planet. Sci.* **37**, 1255 (2002).
27. B. Rava, B. Hapke, *Icarus* **71**, 397 (1987).
28. S. K. Noble, C. M. Pieters, *Astron. Vestnik* **37**, 34 (2003) [English version in *Solar Syst. Res.* **37**, 31 (2003)].
29. M. J. Cintala, *J. Geophys. Res.* **97**, 947 (1992).
30. B. W. Denevi, M. S. Robinson, *Icarus*, 10.1016/j.icarus.2008.04.021 (2008).
31. M. S. Robinson *et al.*, *Science* **321**, 66 (2008).
32. D. L. Domingue *et al.*, *Lunar Planet. Sci.* **39**, abstract 1298 (2008).
33. Some Earth-based reflectance spectra of Mercury show possible evidence of an absorption near 1 μm (1000 nm) attributable to small amounts of ferrous iron in silicates (*3*, *10*, *35*, *36*), whereas others are remarkably featureless (*3*, *9*). Some Earth-based measurements may be affected by interference from Earth's atmosphere.
34. D. T. Blewett, P. G. Lucey, B. R. Hawke, G. G. Ling, M. S. Robinson, *Icarus* **129**, 217 (1997).
35. T. B. McCord, J. B. Adams, *Science* **178**, 745 (1972).
36. T. B. McCord, R. N. Clark, *J. Geophys. Res.* **84**, 7664 (1979).

37. We thank the NASA MESSENGER mission, instrument, planning, and operations teams at the Johns Hopkins University Applied Physics Laboratory and the University of Colorado Laboratory for Atmospheric and Space Physics for support. R. L. McNutt Jr. assisted with mission planning and M. R. Lankton led instrument design. M. Kochte, H. Kang, R. Vaughan, K. Wittenburg, R. Shelton, and A. Berman designed the instrument sequences. The MESSENGER project is supported by the NASA Discovery Program under contracts NAS5-97271 to the Johns Hopkins University Applied Physics Laboratory and NASW-00002 to the Carnegie Institution of Washington.

1 May 2008; accepted 4 June 2008
10.1126/science.1159933